Biomimetics of microducts in three-dimensional bacterial nanocellulose biomaterials for soft tissue regenerative medicine

Osorio, M.; Martinez, E.; Kooten, T. V.; Ganan, P.; Naranjo, T.; Ortiz, I.; Castro, C.

Published in:
Cellulose

DOI:
10.1007/s10570-020-03175-w

Publication date:
2020

Cellulose (2020) 27:5923–5937
https://doi.org/10.1007/s10570-020-03175-w

ORIGINAL RESEARCH

Biomimetics of microducts in three-dimensional bacterial nanocellulose biomaterials for soft tissue regenerative medicine

M. Osorio · E. Martinez · T. V. Kooten · P. Gañán · T. Naranjo · I. Ortiz · C. Castro

Received: 26 November 2019 / Accepted: 20 April 2020 / Published online: 5 May 2020

Abstract The demand for solid organs is increasing worldwide, regenerative medicine aims to develop organs that can replace their human counterparts. In this regard, this study describes a novel biomimetic-based methodology for the incorporation of microducts in 3D bacterial nanocellulose (BNC-3D) biomaterials. Although BNC is a biomaterial that has been used as a scaffold for cell culture purposes, it does not have the microduct structure that solid organs required to maintain cell viability. This study aims to biomimicry the microduct structure (blood vessels) in BNC using a corroded porcine kidney in epoxy resin during BNC synthesis. The resin mold was incorporated into the biological process of producing BNC-3D. After the BNC fermentation, the resin was removed using a novel method (acid hydrolysis) to expose the blood vessels constructs. BNC-3D and BNC-3D with microducts (BNC-3DM) were analyzed using electronic microscopy, infrared analysis, thermogravimetric and biological analysis. Results show that biomaterials biomimicry the blood vessels of the reference organ, moreover, the BNC chemical and morphological properties of BNC was not affected in the biomimetic process. Regarding cell behavior, cell viability was not affected by the incorporation of the microducts, and it was proven that viable cells adhere to the microducts surface, reproducing their shape and migrate into the biomaterial up to 245 μm for 8 days of culture. To conclude, the data demonstrate the potential of biomimetic in BNC for regenerative medicine, in which the microducts transport fluids (blood, nutrients, and waste products) from and to engineered solid organs via animal counterparts.

Electronic supplementary material The online version of this article (https://doi.org/10.1007/s10570-020-03175-w) contains supplementary material, which is available to authorized users.

M. Osorio · E. Martinez · P. Gañán · C. Castro (✉)
School of Engineering, Universidad Pontificia Bolivariana, Circular 1 # 70-01, Medellín, Colombia
e-mail: cristina.castro@upb.edu.co

T. V. Kooten · I. Ortiz
Department of BioMedical Engineering, University Medical Center Groningen, University of Groningen, Antonius Deusinglaan 1, 9713 AV Groningen, The Netherlands

T. Naranjo
School of Health Sciences, Universidad Pontificia Bolivariana, Calle 78B # 72A-109, Medellín, Colombia

T. Naranjo
Medical and Experimental Mycology Group, Corporación Para Investigaciones Biológicas, Carrera 72 A # 78 B-141, Medellín, Colombia

Graphic abstract The graphical abstract represents the structural modification of bacterial nanocellulose (BNC) with the inclusion of microducts and microporosities. Furthermore, it represents the usefulness of the microducts in future applications, where, they can be used for nutrients inlet to feed the cells and to remove the wastes from the developed tissue, same as do the blood vessels.

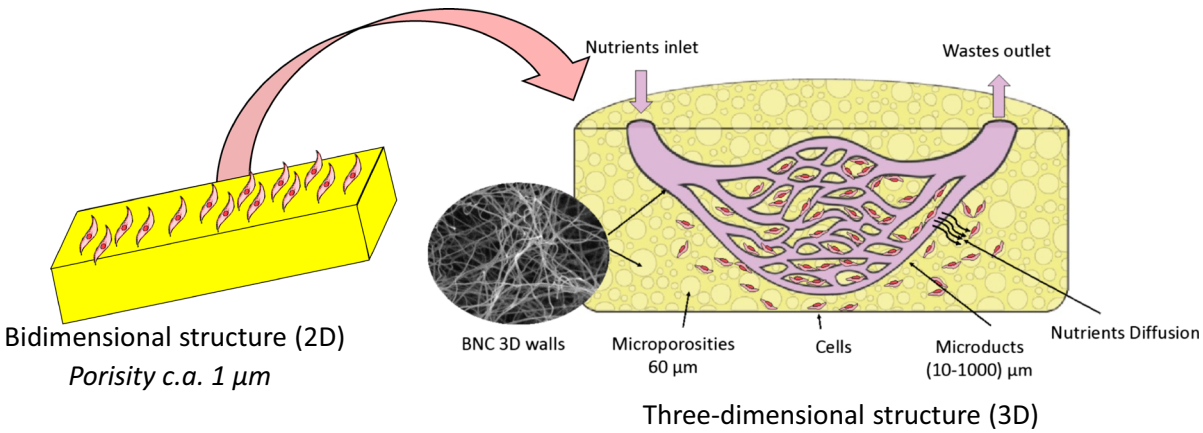

Keywords Bacterial nanocellulose · Biomimetics · Microducts · Regenerative medicine · Three-dimensional biomaterials

Introduction

The demand for solid organs is rapidly increasing worldwide. In the United States, it has been reported that only 7% of patients on the waiting list have received a transplant in 2018 (UNOS 2018). For instance, there are currently nearly 100,000 people on the waiting list for kidney transplantation, with nearly 9000 patients being removed from the list due to deteriorating medical condition or death each year, which reflects the current state of ongoing organ shortage. Despite improved outcomes in renal transplantation, approximately 40% of patients are expected to lose their graft function or die within 10 years (Huling et al. 2019). Furthermore, the transplantation of donated organs is technically challenging because the process depends not only on the availability of the organ but also on factors such as the cost of medical care, infrastructure and equipment availability, and sociocultural and legal factors (Shimazono 2007).

As a result of these difficulties, regenerative medicine aims to find alternatives to meet the high demand for human organs by designing replacements for human counterparts (Murphy and Atala 2014; Bodin et al. 2010). Nevertheless, the human body encompasses complex structures such as different types of cells, proteins, extracellular matrices (ECM), and ducts; these ducts ensure the proper functioning of the other complex structures and transport fluids from, around, and to organ (Góra et al. 2016). In some simple organs, fluids are transported through passive diffusion; however, in solid organs, such as the kidney, liver, or heart, transport through ducts (such as blood vessels, nephrons, and the urinary tract) surrounded by contractile muscles (Góra et al. 2016) becomes necessary.

At the scientific level, the development of scaffold biomaterials that serve as structural framework for the development of organs and tissues (Zhu et al. 2014; Petrochenko et al. 2015; Recouvreux et al. 2011) has been pursued; however, there are few reports that focus on the development of microducts in solid biomaterials. Most of the approaches are focused on the biomimicry of blood vessels, for instance, Gershlak et al. (2017) designed a method for decellularizing spinach leaves to mimic the circulatory system of the heart (Gershlak et al. 2017). Recently, Aydogdu et al. (2019) developed a novel biomimetic small diameter vascular graft using electrospinning of polycaprolactone, ethyl cellulose and collagen type I (Aydogdu

et al. 2019). Likewise, Lei et al. (2019) developed a versatile strategy to fabricate perfusable hierarchical microducts-networks via the combination of one-pot 3D printed sacrificial caramel templates and polymer coating with integrated phase separation. The patterned microducts possess a biomimetic three-level vascular structure including custom-made scalable 3D framework, interconnected microducts and permeable walls with controllable micropores (Lei et al. 2019). However, the methods above do not recreate the whole blood structure of an entire solid organ.

Further efforts for completely biomimicking a solid organ was performed by Huling et al. (2019). They developed a biomimetic renal vascular scaffold based on a vascular corrosion casting technique. Vascular corrosion casts were prepared from normal rat kidneys by perfusion with polycaprolactone (PCL) solution, followed by tissue digestion. The corrosion PCL cast was coated with collagen, and PCL was removed from within the collagen coating, leaving only a hollow collagen-based biomimetic vascular scaffold. The fabricated scaffolds were pre-vascularized with MS1 endothelial cells and subsequently implanted in the renal cortex of nude rats. The implanted collagen-based vascular scaffold was easily identified and integrated into native kidney tissue after 14 implantation days (Huling et al. 2019).

Other approaches based on decellularized animal organs have been developed with the structures present in the original organ in its entirety. Recently, Agarwal et al. (2019) evaluate decellularized caprine liver extracellular matrix (ECM)-based scaffolds for pre-vascularized liver tissue engineering, the results indicated a close similarity of the decellularized matrix to the native liver in terms of its 3D-architecture, mechanical characteristics and ECM composition. Moreover, a significantly higher expression of mature and functional hepatocyte markers was also observed in the decellularized caprine liver ECM as compared to the 2D monolayer control and 2D collagen scaffold. Besides, this 3D scaffolds showed pro-angiogenic properties as confirmed by Chick Chorioallantoic Membrane assay. Upon implantation in a mouse model, the scaffolds did not elicit any significant immunogenic responses (Agarwal et al. 2019). However, the use of human or animal organs seems necessary, wherein the donor's age and the decellularization method may result in the loss of utility of such biomaterials (Courtenay et al. 2017).

According to the above, microducts is a current hot topic in the course for creating laboratory solid organs to meet the demand worldwide as an alternative for transplant. Consequently, in this study bacterial nanocellulose (BNC) aims to biomimicry microduct structures of a solid organ. BNC is an outstanding biomaterial that has been explored for biomedical applications, such as wound dressing, cartilage replacement, artificial substitute for dural defection, among others (Osorio et al. 2019a). In previous in vitro and in vivo studies have shown that this biomaterial can be used to generate three-dimensional microporous structures that allow a high cell infiltrate (Osorio et al. 2018; Osorio et al. 2019a, b). Therefore, this study looks for the incorporation of microducts in 3D BNC (BNC-3DM), using a corroded epoxy resin mold from a pig kidney, which is needed for blood irrigation to guarantee the success of the future implant or solid organ. The biomaterials were morphologically, chemically, thermally, and biologically characterized seeking applications in soft tissue regenerative medicine that to the knowledge of the authors has not been reported previously for nanocellulose.

Materials and methods

Microduct development in BNC

Considering the low viscosity, the development of microducts via biomimetics involved the use of epoxy resin-plastinated molds, thereby facilitating resin migration through the organ's microducts, as well as the copy of structures at the micrometric scale (von Hagens 1979; Hagens et al. 1987). A porcine kidney was selected as the model because of its similarities with the human kidney and its previous use as an animal model to study kidney failure (Giraud et al. 2011).

The methodology for developing the biomaterials is shown in Fig. 1. A fresh porcine kidney donated by a local butcher's shop was washed using plenty saline solution and metal catheters to remove coagulated blood. Further, Smooth-on® epoxy resin was prepared by following the manufacturer's guidelines in 10% w/w methylethyl ketone. Then, 50 mL of the mix was injected into the porcine kidney's renal vein and artery, which were then rapidly sealed with an umbilical cord clamp to prevent resin backup. The

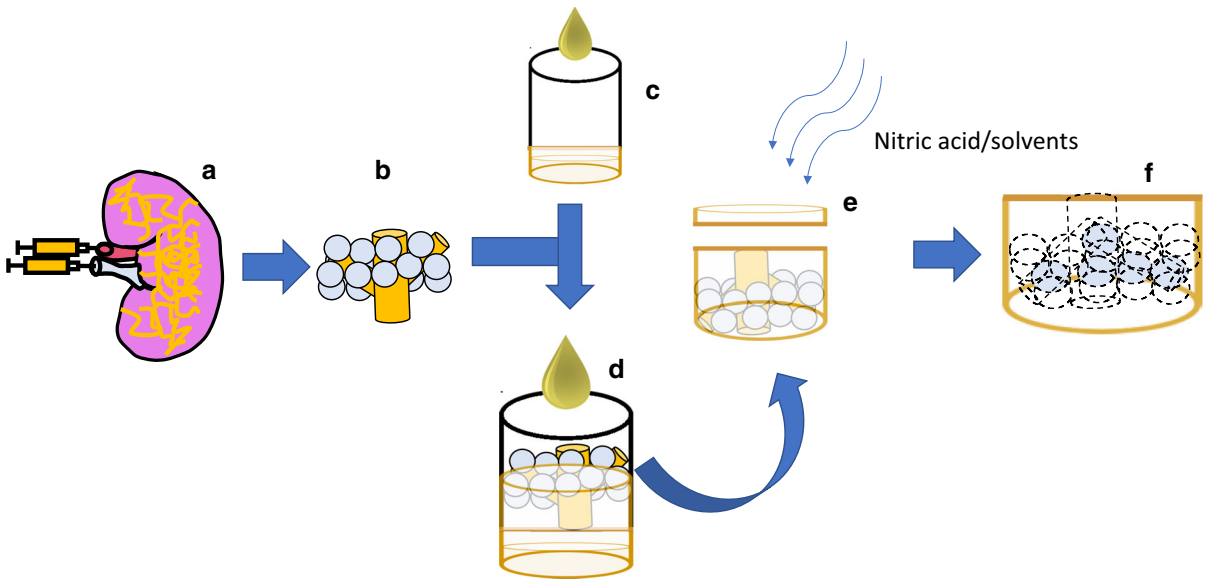

Fig. 1 Process for developing microducts in BNC-3D: **a** plastination of a pig kidney using epoxy resin; **b** microducts and microspheres mold; **c** production of a first BNC layer; **d** growing of BNC in the molds; **e** mold removing using nitric acid 4 M and solvents; **f** final biomaterial

resin was cured for 24 h at 4 °C (see Fig. 1a). Next, the organ was corroded using a 40% w/w NaOH solution for 48 h. Later, the resin pre-mold was thoroughly washed with distilled water to obtain a neutral pH and remove the NaOH. Finally, it was frozen at − 80 °C and freeze-dried under 0.020 mBar vacuum pressure and mixed with 0.5 g of paraffin microspheres (PMS) (see Fig. 1b).

BNC was synthesized using the methodology of Osorio et al. (2017), briefly, in a 12 well cell culture plate, in which 1 mL of Hestrin–Schramm culture media at pH ca. 3.6, inoculated with *Komagataeibacter medellinensis* was added and incubated for 3 days to generate the first BNC layer (Osorio et al. 2018) (see Fig. 1c). Further, the positive resin epoxy mold and 0.5 g PMS of a diameter of 61.24 (12.04) µm were placed. Every 3 days 200 µL of fresh growth medium were added until the whole mold was covered with BNC (see Fig. 1d). At the end of the fermentation, the biomaterials were of 1 cm thickness.

To generate the microducts the epoxy resins should be removed from BNC-3D, the resin microstructures were removed using 4 M nitric acid solution at 85 °C for 5 h, followed by washing with water at 80 °C until the resin was completely removed. Subsequently, the biomaterial was subjected to the PMS removal process, as described by Osorio et al. (2018), briefly, the samples were dehydrated using ethanol, then it was subjected to cycles with xylol, ethanol and water (see Fig. 1e). The detailed protocol can be reviewed in the following reference (Osorio et al. 2018). The Fig. 1f shows the final state of the biomaterials, a BNC 3D structure with void spaces, representing microporosities and microducts.

Characterization of 3D BNC biomaterials with microducts

Scanning electron microscopy (SEM)

SEM was used to assess the morphology of the mold of microducts and 3D biomaterials with and without microducts (BNC-3D and BNC-3DM). The samples were frozen at − 196 °C using liquid nitrogen and freeze-dried to be subsequently coated with gold. Samples were observed using a Jeol JSM 5910 LV scanning electron microscope at 20 kV. To measure blood vessel diameters, SEM images were calibrated in ImageJ2® (Rueden et al. 2017) using the scale bar, then the diameter was determined using line tools.

Attenuated total reflectance-Fourier transform-infrared spectroscopy (ATR-FTIR)

ATR-FTIR was performed to examine the residual presence of compounds used throughout the process, such as paraffin and epoxy resin, as well as to detect potential changes in the chemical and crystalline structure of the BNC. Before the analysis, five samples were gravimetrically oven-dried at 105 °C. Experiments were conducted using an FTIR spectrometer (Nicolet 6700 Series) equipped with the ATR accessory, which comprises a Type IIA diamond crystal mounted in tungsten carbide. The sampling area was approximately 0.5 mm^2; constant and reproducible pressure was applied for each sample. The infrared spectra were collected at a resolution of 4 cm^{-1} over 64 scans.

The content of allomorphisms Iα and Iβ in BNC was calculated using the correlation reported by Imai and Sugiyama (1988), as a function of the area (A) of the absorbance peaks at 710 cm^{-1} and 750 cm^{-1} bands according to Eq. 1. (Imai and Sugiyama 1998). Areas were measured based on a standard spectra using Omnic™ (Thermofisher) software and its mathematical tools.

$$I\alpha = \frac{A_{750}}{(A_{750} + 0.16A_{710})} \quad (1)$$

X-ray diffraction (XRD)

X-ray diffraction was conducted to analyse the effect of the described methods on the BNC crystallinity. Three oven-dried biomaterials per method were X-rayed using an XPert PANalytical Empyrean II-Alpha1 diffractometer operating at a Kα1/Kα2 ratio of 0.5 with a radiation wavelength of 1.542 Å. Data were collected in reflection mode in the 5–60° range with a step of 0.026°. The scans preceded at 51.765 s per step. The diffraction peaks were fitted using pseudo-Voigt and Gaussian functions. The crystallinity index (Cr.I) was calculated according to Molina-Ramirez et al. (2017) as the percentage of the area of all crystalline peaks to the total area (Molina-Ramirez et al. 2017). The d-spacing (d) between the crystal planes was determined using Bragg's law expressed by Eq. (2):

$$d = \frac{\lambda}{2sin\theta} \quad (2)$$

where θ is the angle between the plane and the diffracted or incident beam and λ is the wavelength of the X-rays. An apparent crystal size (ACS) approximation was calculated using Scherrer's formula (Eq. (3)):

$$ACS = \frac{0.9\lambda}{FWHMcos\theta} \quad (3)$$

where the FWHM is the width of the peak at half of the maximum height, θ is the Bragg's angle, and λ is the wavelength of the X-rays. Three samples of BNC-3D and BNC-3DM were used for the analysis.

Thermogravimetric analysis (TGA)

Potential changes in the thermal properties of 3D biomaterials during processing were assessed using a thermogravimetric analyzer (Mettler Toledo TGA/SDTA 851E). Further, 8 mg of dry sample with and without microducts was weighed; the assay was conducted in a nitrogen atmosphere, within a temperature range between 30 and 800 °C, with a heating rate of 10 °C min^{-1}.

XTT cell viability assay

A total of 25,000 viable fibroblasts were inoculated in a 12-well culture box containing each 3D BNC biomaterial (with and without microducts). Cells were incubated for 8 days with 10% SBF-DMEM supplemented by 1% penicillin–streptomycin. Then, materials were extracted and placed in a new box with 50 µL of activated XTT and 500 µL of culture medium. Samples were incubated for 3 h at 37 °C in a 5% CO_2 atmosphere. At the end of this period, 100 µL of the sample was transferred to a 96-well plate and absorbance was recorded at 485 nm (reading) and 690 nm (reference) using a Fluostar Optima multimode microplate reader. Finally, to estimate cell viability, the reference value was subtracted from the reading value. The experiment was performed at 5 different moments.

Confocal microscopy

Confocal microscopy was used to visualize the cells adhered to BNC-3D and BNC-3DM biomaterials. After 8 days of culture, fibroblasts were fixed using 3.7% v/v formaldehyde for 30 min. They were then washed with PBS, and the cell membrane was removed using 0.01% v/v Triton X-100. Cells were blocked with a 5% v/v solution of BSA for 30 min and marked for fibronectin with Rabbit anti-fibronectin (first antibody) to mark the cell's cytoskeleton. Next, the cells in the biomaterial were washed with 1% v/v BSA and PBS and then marked using RedX Donkey anti-Rabbit IgG and DAPI (secondary antibody). The excess dye is removed by successive washes with 1% v/v BSA and PBS. Cells were visualized with a Leica TCS SP2 confocal microscope at an excitation wavelength of 573 nm and 358 nm for fibronectin and the core, respectively. Images were collected, forming a z-stack through a depth up to 245 µm in the biomaterial. Core and fibronectin images were individually taken and later combined using ImageJ2® (Rueden et al. 2017).

Statistical analysis

Statistical analysis was conducted to determine significant differences. One-way ANOVA was used for crystallinity and cell viability assays. All experimental data met the homoscedasticity and normality assumptions. A p value < 0.05 was considered statistically significant. Standard deviations are shown in brackets next to the average of the variable.

Results

Biomimetics of microducts in 3D BNC biomaterials

Figure 2 shows a photograph of the microducts of a porcine kidney plastinated in epoxy resin. The resin imitated the organ's external (see Fig. 2a) and internal (see Fig. 2b) fibril structures, which are connected to the blood vessels of the renal cortex (Gueutin et al. 2012). The renal vein and artery can also be observed, as indicated by arrows in Fig. 2b.

Figure 3 shows in further detail these microducts. They possess a high size distribution, with diameters above 500 µm in the renal artery or vein. Diameters below 10 µm were found for the glomeruli and their afferent and efferent arterioles. However, by the diameter distribution (Fig. 3a), over 60% of them range from 10 to 100 µm, with an average of 43.0 (23.5) µm. This corresponds to the segmentation of renal arteries and veins into interglobular vessels, which are smaller in diameter and greater in number (Fig. 3c, d, and e). Furthermore, it was observed in the vessel surface (Fig. 3b) that the epoxy resin was able to biomimicry the roughness and grooves of the blood epithelia (Gueutin et al. 2012; Levey et al. 2005).

The above results make it possible to assert that the plastination method is highly accurate because it allowed the biomimetic of the anatomy of the kidney's blood vessels and arterioles.

After checking that the mold had the appropriate microstructure, it was used to produce microducts in the 3D BNC biomaterial. Figure 4 shows the micrographs of the biomaterial after BNC synthesis. It can be observed that *K. medellinensis* is able of producing BNC in the free spaces left by the epoxy resin and PMS (see Fig. 4a), thus generating a biomaterial with 3D structures and microducts (BNC-3DM).

Figure 4b–e show different images of the BNC-3DM after the epoxy resin and paraffin removal process. In this figure, microducts and microporosities can be observed (indicated by arrows and triangles, respectively) in the biomaterial. It can be noted that microporosities are connected by microducts, which would make cell and nutrient migration toward the core of the biomaterial easier. Further, this would facilitate tissue development, in the first instance, and fluid distribution (blood) within the biomaterial, in the second instance, to provide cells with nutrients and allow the removal of waste products (Murphy and Atala 2014; Góra et al. 2016).

As explained previously, the process to remove the epoxy resin from BNC-3DM demands the use of a 4 M nitric acid solution and this can induce negative effect on the BNC microstructure (morphology and crystallinity), chemistry or thermal properties. Consequently, BNC-3D and BNC-3DM were investigated using SEM, FTIR and TGA to address possible changes in the BNC properties. Figure 5 shows images at high-magnification SEM to whether or not the nitric acid process generates changes in the BNC nanoribbons.

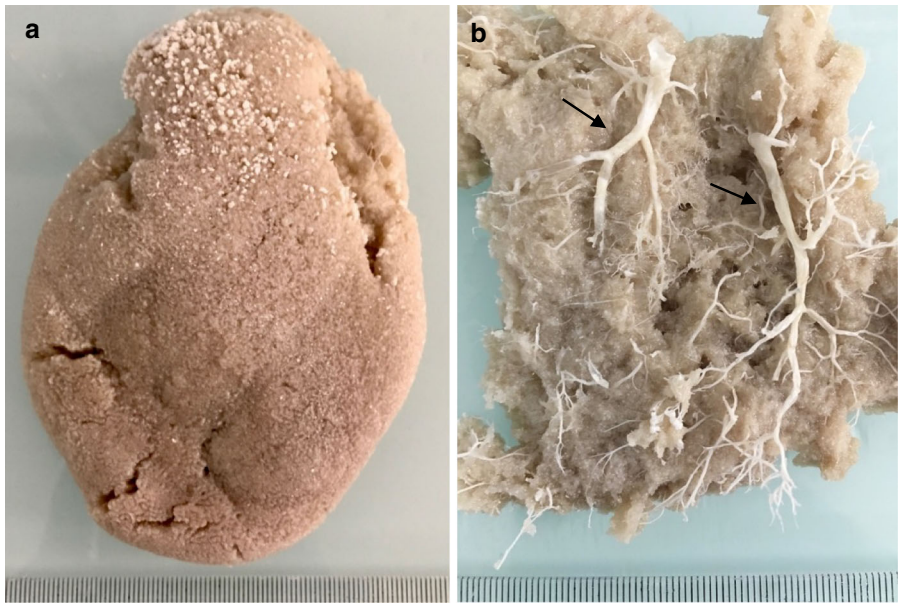

Fig. 2 Plastinated porcine kidney: **a** Macroscopic photograph of the outer part of the kidney. **b** Macroscopic photograph of the inner part of the kidney. The images represent a width of 10 cm

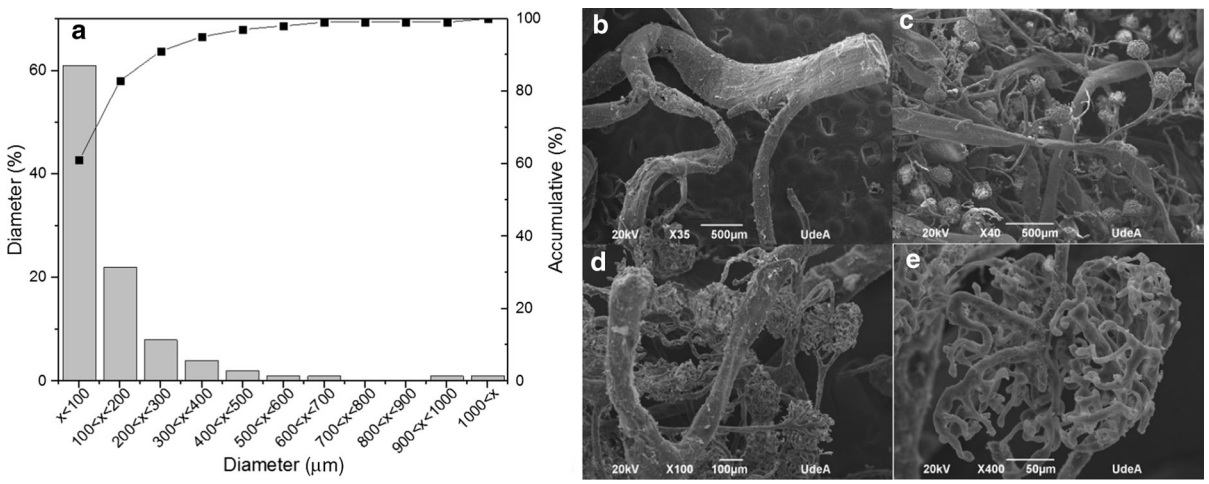

Fig. 3 Distribution of the diameters of microducts and SEM images at different magnification levels. **a** Diameter distribution. SEM images. **b** 35x, the scale represents 500 μm; **c** ×100, the scale represents 100 μm; **d** ×40, the scale represents 500 μm; **e** ×400, the scale bar represents 50 μm

Figure 5 shows that the interconnected network of BNC nanoribbons is preserved after treatment with nitric acid; in both cases, a network of randomly arranged nanoribbons was observed, with a porosity between ribbons of around 1 μm (Feldmann et al. 2013; Gama et al. 2013). This network is highly important to preserve the biomaterial mechanical properties. In biomedicine, it has been widely argued that this microstructure imitates the collagen network of the extracellular matrix (Gama et al. 2013; Iguchi et al. 2000); therefore, it needs to be preserved to avoid affecting the biomaterials' biological properties. The following section discusses the effect of this process on the BNC chemical and crystalline structure.

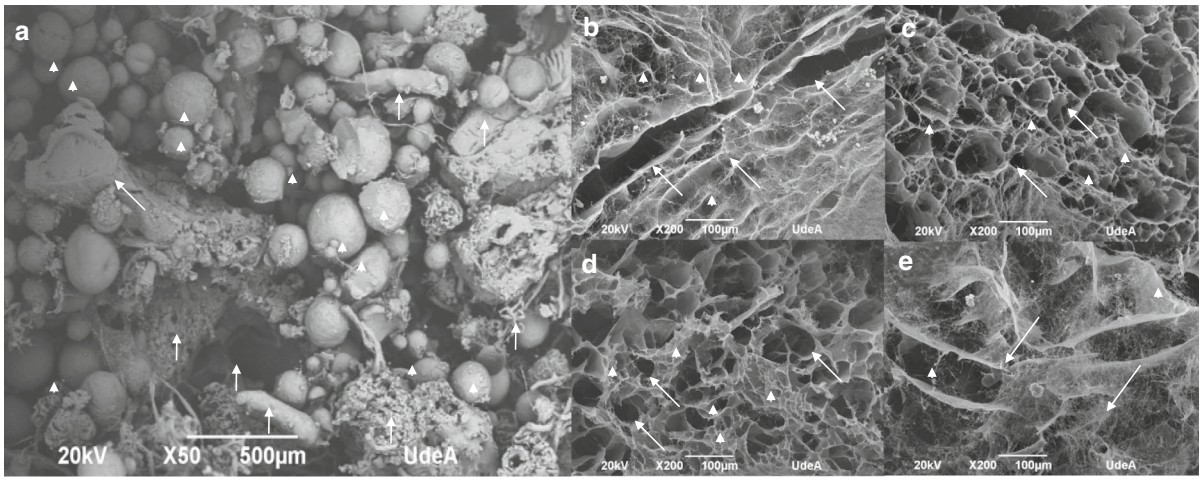

Fig. 4 PMS and microducts premold and BNC-3D with microporosities and microducts. **a** SEM of the PMS (arrowhead) and microducts premold (arrow) at ×50, the scale represents 500 µm; **b–e** Microstructure of BNC-3DM biomaterials with microporosities (arrowhead) and microducts (arrows). SEM images taken at ×200; the scale length is 100 µm

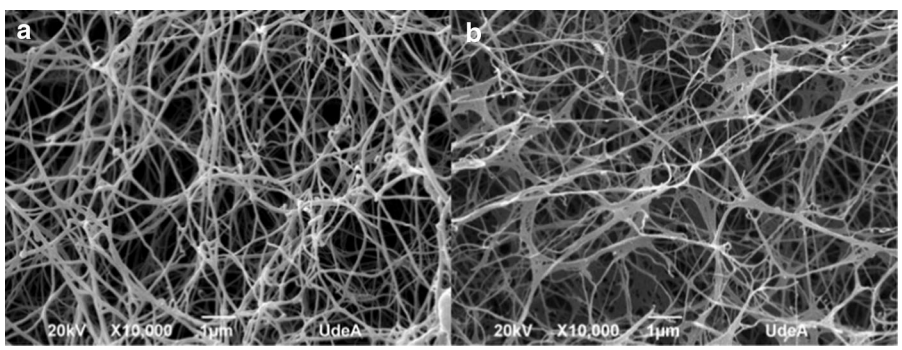

Fig. 5 High-magnification BNC nanorribbons; **a** 3D BNC image taken at ×10,000; the scale length represents 1 µm; **b** BNC-3DM image taken at ×10,000; the scale bar represents 1 µm

Chemical and crystallinity analysis of BNC-3D and BNC-3DM

FT-IR and XRD was performed to find changes in the biomaterials' chemical and crystalline structure. The results are shown in Fig. 6.

In accordance with Fig. 6a, neither NO_2 groups (associated to possible surface modifications of cellulose to nitrocellulose due to reaction with nitric acid) related to vibrational bands at 1573 and 1383 cm^{-1} (Su et al. 2015; de la Ossa et al. 2012), nor groups concerning epoxy resin (vibrations at 1613, 1500, or 818 cm^{-1}) (Li et al. 2015) were identified in the spectrum of 3D Micro-BNC biomaterials. The study also found no evidence of vibrations from paraffinic hydrocarbons (sharp peaks at 2917, 2849, 1463, and 719 cm^{-1}) (Wang et al. 2010). The spectra obtained both for the 3D Micro-BNC and 3D BNC biomaterials are dominated by type-I cellulose vibrational peaks (Chiaoprakobkij et al. 2011; Yan et al. 2008; Shi et al. 2012; Kim et al. 2011; Castro et al. 2012), i.e., vibrations around 3348 cm^{-1} were attributed to the stretching of the OH group. In addition, absorption bands at 2894, 1428, and 1062 cm^{-1} were attributed to the stretching of groups C–H of $–CH_2$, the symmetrical bending of $–CH_2$ group, and the vibrations of the C–O–C groups of pyranose rings, respectively (Amin et al. 2014). Other bands at 1374 cm^{-1}, 1337 cm^{-1}, and 1315 cm^{-1} were attributed to bending of the C–H groups, plane bending of the O–H group, and bending of the CH_2 group, indicating the presence of crystalline regions within the BNC structure (Castro et al.

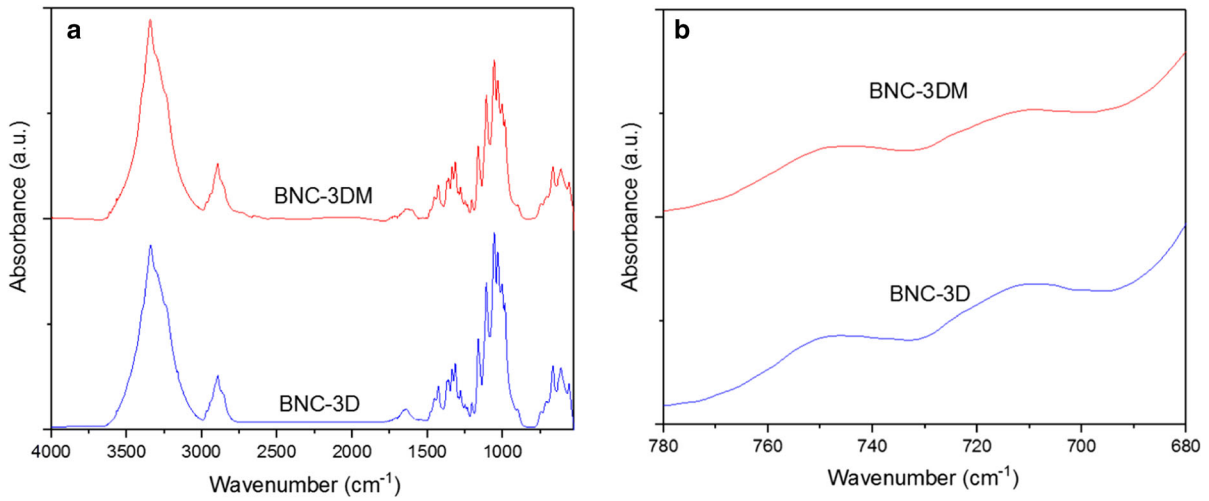

Fig. 6 BNC chemical and crystallinity analysis. **a** ATR-FTIR spectra; **b** approach to the area between 780 and 680 cm^{-1} of the ATR-FTIR spectra

2012). The 750 and 710 cm^{-1} bands (see Fig. 5b) are associated with the presence of crystalline allomorphisms Iα and Iβ. In both biomaterials, regions, rich in Iα cellulose, were found with a rate of 0.879 (0.030), similar to the findings by other authors regarding BNC (Castro et al. 2011).

Finally, the crystallinity percentage, d-spacing and the apparent crystal size (ACS) were calculated using X-ray diffraction, the analysis is shown in the Fig. 7. d-spacing and apparent crystal size (ACS) are presented in Table 1.

This study showed that for BNC-3DM biomaterial, (compared with BNC-3D biomaterial), treatments using nitric acid resulted in no changes in the BNC crystallinity or crystal size dimension. The above-mentioned behavior was attributed to the treatment with 4 M nitric acid, which was not strong enough to depolymerizes or erode the crystalline or amorphous regions of BNC. These results are in agreement with Huntley et al. (2015), in which they found that to affect the cellulose crystallinity with nitric acid, the concentration should be above 5 M (32% w/v) (Huntley et al. 2015). Moreover, it is not aggressive enough to

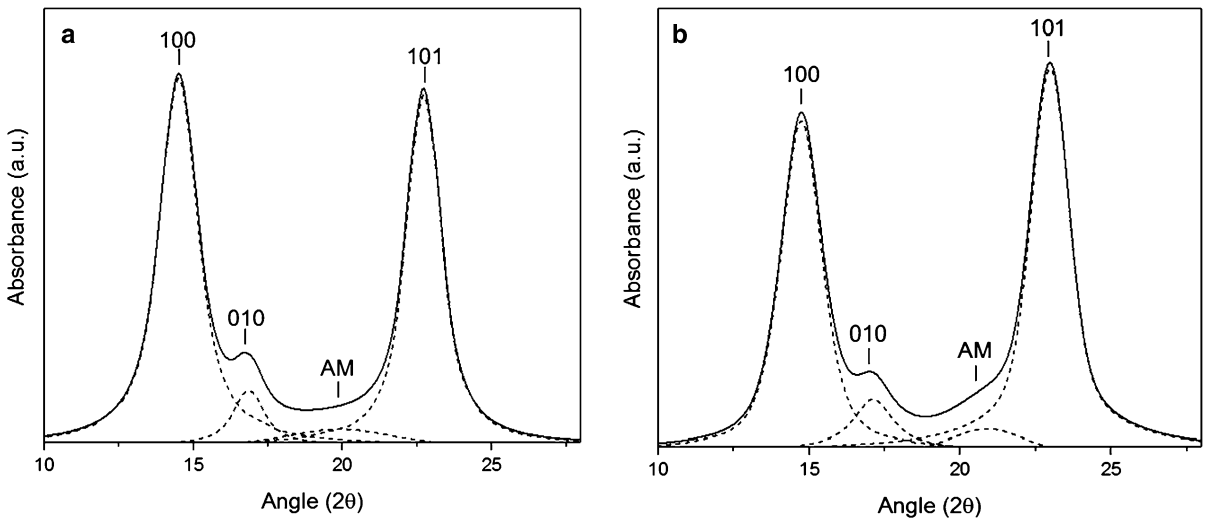

Fig. 7 X-ray difractogram of the biomaterials, **a** BNC-3D and **b** BNC-3DM

Table 1 X-ray parameters size of biomaterials BNC-3D and BNC-3DM

Crystalline plane	X-ray parameter % crystallinity	BNC-3D 96.50 (1.03)	BNC-3DM 97.16 (2.10)
100	d (nm)	0.31 (0.00)	0.30 (0.00)
	ACS	5.33 (0.17)	5.14 (0.77)
010	d (nm)	0.26 (0.00)	0.26 (0.00)
	ACS	5.99 (0.80)	6.41 (2.56)
101	d (nm)	0.20 (0.00)	0.20 (0.00)
	ACS	6.09 (0.05)	6.07 (1.25)

destroy the BNC nanoribbons morphology (as observed in Fig. 5) and it was effective to remove the epoxy resin. Comparing the crystalline parameters presented in the Table 1. with those where was used the same BNC sources (BNC produced by *Komagataeibacter medellinensis*) reported in the literature, there were no differences in the % crystallinity, ACS nor d-spacing, meaning that the process of creating microporosities and microducts has no negative influence in the BNC crystallinity (Osorio et al. 2018).

Thermal analysis of 3D BNC biomaterials with microducts

Finally, to investigate possible changes in the BNC thermal properties by nitric acid treatment. TGA analysis was conducted. Figure 8 shows the TGA and DTG curves for the 3D BNC and 3D Micro-BNC biomaterials.

The above figure shows that the biomaterial keeps its natural thermal stability after its treatment with nitric acid to remove the epoxy resin. Both biomaterials performed an onset decomposition temperature of 280 °C and a maximum decomposition rate of 2.5E-03%/min. As a consequence of no change of the chemical nor crystalline structure of BNC, the thermal properties of BNC remained unchanged (George et al. 2011; Isogai 2013).

Cell studies in 3D micro-BNC

To conclude this first approach to the development of microducts in 3D BNC, cell viability in 3D Micro-BNC biomaterials was assessed (Fig. 9).

According to Fig. 9, the epoxy resin removal process of microducts has no negative influence on cell viability. After 8 days of culture, cells exhibit cellular respiration and are able of reducing tetrazolium salts to formazan. Furthermore, no statistically significant differences were found regarding viability between BNC-3D and BNC-3DM. Both biomaterials supported cellular adhesion (see Fig. 9b and c). This confirms that after removing the paraffin and epoxy resin, no toxic components that may have prevented adhesion or generated cell damage in BNC remains. On the other hand, the material now possesses the

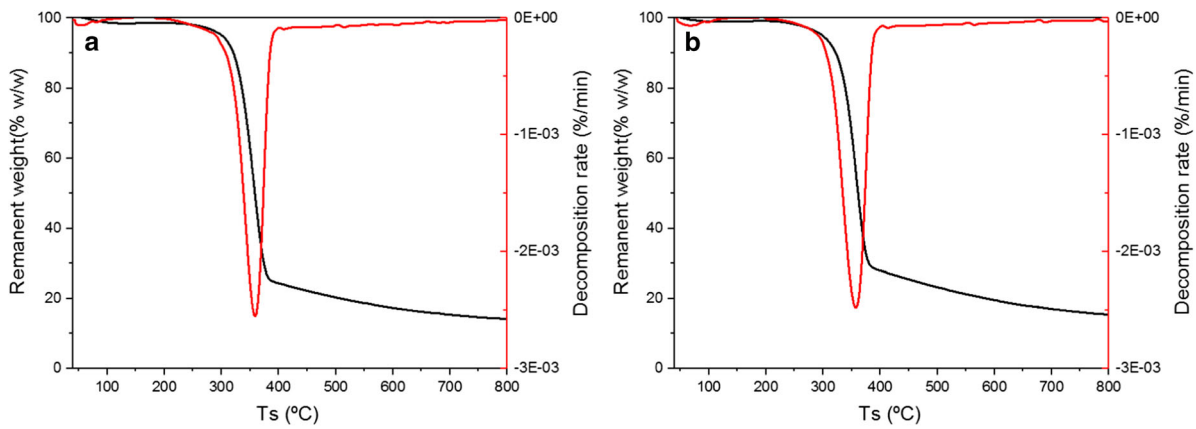

Fig. 8 Thermogravimetric analysis of biomaterials; **a** TGA and DTG curves for BNC-3D, TGA, and **b** DTG curves for BNC-3DM

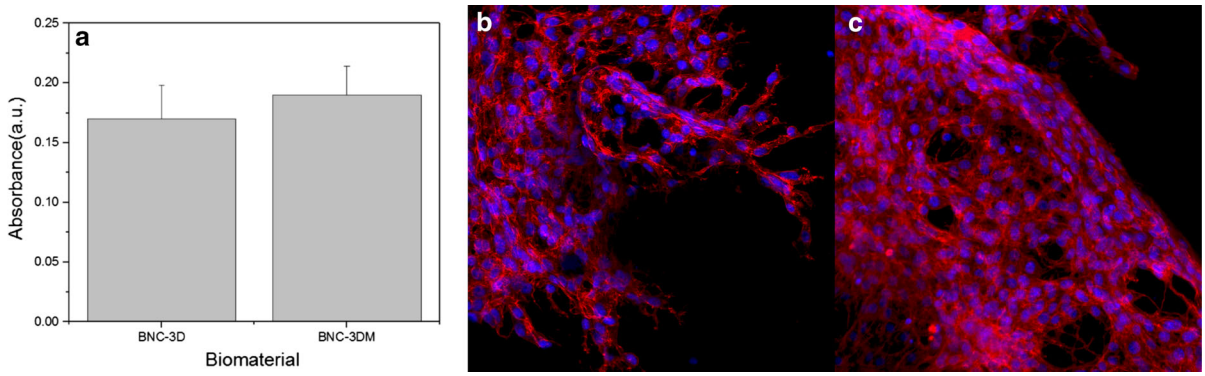

Fig. 9 Cell studies conducted on 3D BNC and 3D Micro-BNC biomaterials; **a** XTT viability assay; **b** cells in 3D BNC (150 μm in depth); image width represents 375 μm; **c** cells in 3D Micro-BNC (150 μm in depth); image width represents 375 μm

microducts that allow tissue regeneration, in which the presence of them will allow the transport of blood with nutrients and oxygen to prevent apoptosis or necrosis in the implanted tissue (Rouwkema et al. 2008).

To specify the presence of microducts in the biomaterial, multiple fields were explored, in which it was possible to detail the cellular morphology surrounding them (Fig. 10).

Cells were aligned in the microducts' walls and capable of proliferating throughout their length (Fig. 10c). Likewise, it could be observed that cells homogeneously coated the microduct's walls without losing their cellular morphology. This could be highly significant for the design and regeneration of capillary vessels in solid organs, where smooth muscle cells regenerating the organ's blood vessels could be cultivated over the first fibroblast support layer (Acosta Gómez 2006).

Discussion

Currently, the development of microducts in biomaterials for tissue regeneration is one of the challenges faced by scientists who seek to imitate the structures of human organs and tissues, the lack of a viable vascular network is limiting the application of 3D scaffolds or constructs in clinical practice (Gershlak et al. 2017). The morphology of the solid organ microducts is complex, has no symmetry axes, is highly branched, and has diameter dispersion from centimeters up to several microns (Gao 2017). The complexity of these systems results in the failure of rapid prototyping techniques (such as 3D printing) because they do not have the appropriate resolution to imitate the branches of lower diameter, such as capillary vessels (Do et al. 2015), ending in structures dimensionally simple formed by geometric arrangements, such as square-based pyramidal constructions (Yeong et al. 2010). These are far from the structures actually found in the human body.

Conversely, organ and tissue plastination are techniques that have allowed the imitation of animal structures with a high degree of reliability (Hagens et al. 1987). However, their use has been set aside for educational purposes. This study proposes the use of this technique to biomimicry the structures of animal organ microducts, similar to human ones, to subsequently perform biomimetics using BNC. Despite the plastination potential, these techniques are rarely reported because many scientists do not consider it as a science (Kc et al. 2007). However, in this study, the imitation of the blood vessels morphology, including large renal arteries and veins and nephron arterioles with diameters of around 10 μm, was achieved through the use of low viscosity epoxy resin, and on the basis of the results of this study (as shown in Figs. 2 and 3). Furthermore, the fermentation process was adapted to reproduce a 3D bioprinting, in which, can be reproduced the better conditions to prevent BNC delamination (Osorio et al. 2018), just 200 μL were used every 3 days for promoting a denser and compact BNC production as the low volume will keep the new bacterium generation closer to maintain the BNC ribbons interconnection. Likewise, at the 3rd day the strain is in its exponential growth (Molina-Ramirez et al. 2017), allowing a rapid population of the added volume. Accordingly, this technique was

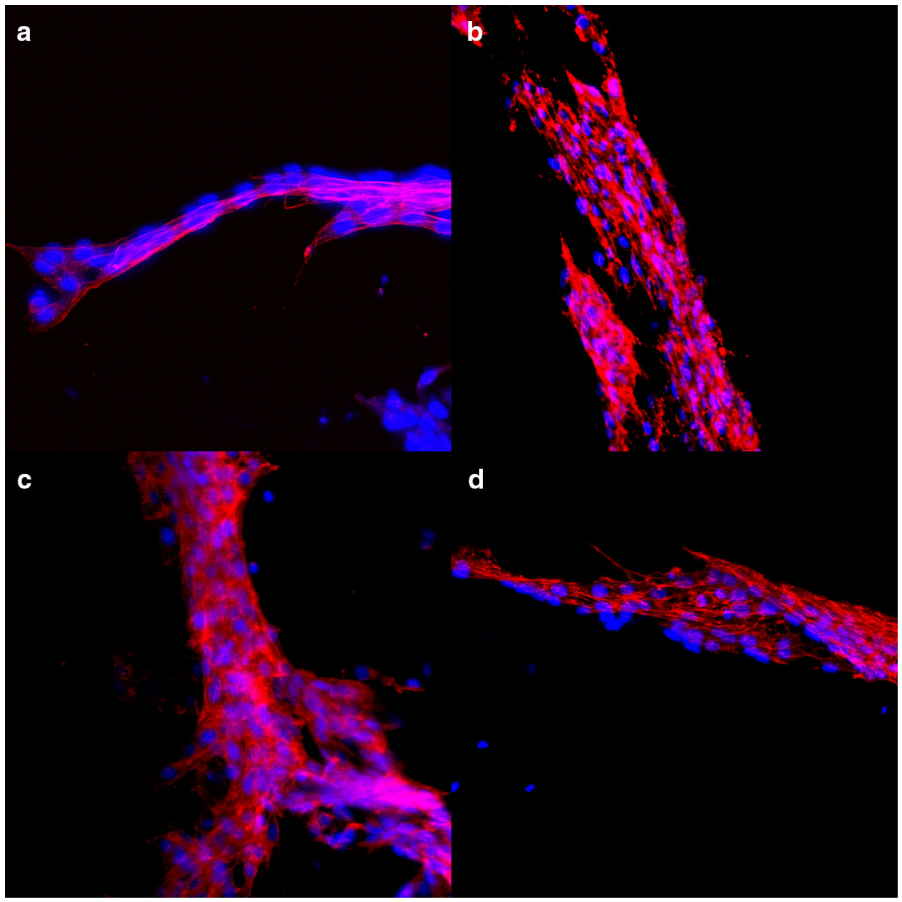

Fig. 10 Detailed microducts in 3D Micro-BNC; **a–d** images taken at ×63; image width represents 375 µm

considered appropriate to imitate the structures of solid organs' microducts to biomimicry that morphology in BNC, which is novel for this biomaterial.

The next challenge was faced during the removal of epoxy resin from BNC to leave the microducts behind. Epoxy resin is a thermosetting polymer of high chemical and thermal stabilitty (Li et al. 2015; Davoodi et al. 2012); therefore, the problem of removing resin without negatively affecting BNC's properties arose. However, it was found that epoxy resin may depolymerize with the help of concentrated nitric acid solution (4 M), which breaks the resin chains at carbon among the bisphenol groups (Dang et al. 2002, 2005). However, this treatment may also result in the nitration of lateral groups in BNC (producing nitrocellulose), depolymerization the BNC chains, or amorphization the biomaterial (Cui et al. 2014; Su et al. 2015), which would lead to changes in the chemical, crystalline, and morphological structure of BNC that would reduce its applicability in regenerative medicine.

Morphologically, after the nitric acid process, there were no changes either in the diameters of nanoribbons or network configuration. In contrast, the resin could be completely removed, exhibiting the tubular structures of microducts in the biomaterial. The chemical analysis did not show the presence of nitro groups bands in BNC-3DM biomaterials, which would allow to assert that under these conditions, nitric acid reacts easier with the epoxy resin rather than with BNC. The chemical structure of the epoxy resin has two attracting electron effects resulting from the presence of bisphenol groups in its chains, facilitating the nitric acid attack and subsequent chain breakdown (McMurry 2004). BNC does not have groups producing such effects; thus, a stronger acid catalyst would be required to start the reaction of the nitric acid with BNC (Sullivan et al. 2018). The above was

demonstrated here using SEM, FTIR, XRD and TGA, these techniques confirmed that morphology, the chemical structure, the crystallinity and the thermal properties of BNC were unchanged.

Finally, to validate the methodology of developing microducts in BNC the biomaterial was seeded with 25,000 fibroblasts for 8 days fibroblasts. It was found that BNC-3DM allows cell adhesion and spreading without causing cell apoptosis. Supplementary information (S.I.1) shows a video of z-stack of confocal images, the images were taken from the surface of the biomaterial up to 245.7 µm of depth with a step of 6.3 µm. In the video can be seen the infiltration of the cells in the biomaterial and how the cells, at 8th culture time, adheres the microduct walls, imitating their shape, and then to the microporous without losing their cell morphology.

The above results indicate the feasibility of designing microducts in BNC biomaterials using a biomimetic approach throughout BNC biosynthesis using a corroded epoxy resin mold from a pig kidney. These novel microducts can be used for transporting fluids from and into BNC. This is a first step in the biomimetics of microducts in solid organs based on equivalent animal organs, for future applications in soft regenerative medicine of solid organs.

Conclusions

In this paper, a biomimetic methodology for designing microducts in BNC-3D was developed. The approach used a plastinated microducts from an animal equivalent. Moreover, this paper proposes a new method to remove epoxy resin from BNC that does not affect the BNC properties, which are crucial for biomedical applications. The BNC-3DM biomaterials showed microducts at low magnifications, and at high magnifications no changes were observed in the biomaterial nanoribbons network. Furthermore, there were no changes in the BNC functional groups, crystallinity and onset temperature. Regarding cell behavior, cell viability was not affected by the microducts. Moreover, it could be proven that cells adhere to the surface of microducts, imitating their shape throughout their length. To implement the use of these biomaterials in future kidney transplants, further studies are needed to focus on cultivating endothelial cells in these biomaterials and conducting an in-depth analysis on the nephron filtration process and the way to biomimicry this process using BNC.

Acknowledgments Authors wants to acknowledgement to COLCIENCIAS (NanoBioCáncer Grand Number FP44842-211-2018) and to CIDI-UPB for the funding that allowed the realization of this work. Moreover, the authors would like to thank the Ibero-American Program of Science and Technology for Development (CYTED Networks).

References

Acosta Gómez AP (2006) El fibroblasto: su origen, estructura, funciones y heterogeneidad dentro del periodonto. Univ Odontol 25:26–33

Agarwal T, Maiti TK, Ghosh SK (2019) Decellularized caprine liver-derived biomimetic and pro-angiogenic scaffolds for liver tissue engineering. Mater Sci Eng C 98:939–948. https://doi.org/10.1016/j.msec.2019.01.037

Amin MC, Abadi AG, Katas H (2014) Purification, characterization and comparative studies of spray-dried bacterial cellulose microparticles. Carbohydr Polym 99:180–189. https://doi.org/10.1016/j.carbpol.2013.08.041

Aydogdu MO, Chou J, Altun E et al (2019) Production of the biomimetic small diameter blood vessels for cardiovascular tissue engineering. Int J Polym Mater Polym Biomater 68:243–255. https://doi.org/10.1080/00914037.2018.1443930

Bodin A, Bharadwaj S, Wu S, Gatenholm P, Atala A, Zhang Y (2010) Tissue-engineered conduit using urine-derived stem cells seeded bacterial cellulose polymer in urinary reconstruction and diversion. Biomaterials 31:8889–8901. https://doi.org/10.1016/j.biomaterials.2010.07.108

Castro C, Zuluaga R, Putaux JL, Caro G, Mondragon I, Gañán P (2011) Structural characterization of bacterial cellulose produced by *Gluconacetobacter swingsii* sp. from Colombian agroindustrial wastes. Carbohydr Polym 84:96–102. https://doi.org/10.1016/j.carbpol.2010.10.072

Castro C, Zuluaga R, Álvarez C, Putaux JL, Caro G, Rojas OJ, Mondragon I, Gañán P (2012) Bacterial cellulose produced by a new acid-resistant strain of Gluconacetobacter genus. Carbohydr Polym 89:1033–1037. https://doi.org/10.1016/j.carbpol.2012.03.045

Chiaoprakobkij N, Sanchavanakit N, Subbalekha K, Pavasant P, Phisalaphong M (2011) Characterization and biocompatibility of bacterial cellulose/alginate composite sponges with human keratinocytes and gingival fibroblasts. Carbohydr Polym 85:548–553. https://doi.org/10.1016/j.carbpol.2011.03.011

Courtenay JC, Johns MA, Galembeck F, Deneke C, Lanzoni EM, Costa CA, Scott JL, Sharma RI (2017) Surface modified cellulose scaffolds for tissue engineering. Cellulose 24:253–267. https://doi.org/10.1007/s10570-016-1111-y

Cui Q, Zheng Y, Lin Q, Song W, Qiao K, Liu S (2014) Selective oxidation of bacterial cellulose by NO_2-HNO_3. RSC Adv 4:1630–1639. https://doi.org/10.1039/C3RA44516J

Dang W, Kubouchi M, Yamamoto S, Sembokuya H, Tsuda K (2002) An approach to chemical recycling of epoxy resin

cured with amine using nitric acid. Polymer 43:2953–2958. https://doi.org/10.1016/S0032-3861(02)00100-3

Dang W, Kubouchi M, Sembokuya H, Tsuda K (2005) Chemical recycling of glass fiber reinforced epoxy resin cured with amine using nitric acid. Polymer 46:1905–1912. https://doi.org/10.1016/j.polymer.2004.12.035

Davoodi MM, Sapuan SM, Ahmad D, Aidy A, Khalina A, Jonoobi M (2012) Effect of polybutylene terephthalate (PBT) on impact property improvement of hybrid kenaf/-glass epoxy composite. Mater Lett 67:5–7. https://doi.org/10.1016/j.matlet.2011.08.101

de la Ossa MAF, Torre M, García-Ruiz C (2012) Nitrocellulose in propellants: characteristics and thermal properties. Advances in Materials Science Research. Nova Science Publishers, Hauppauge

Do AV, Khorsand B, Geary SM, Salem AK (2015) 3D printing of scaffolds for tissue regeneration applications. Adv Healthc Mater 4:1742–1762. https://doi.org/10.1002/adhm.201500168

Feldmann EM, Sundberg JF, Bobbili B, Schwarz S, Gatenholm P, Rotter N (2013) Description of a novel approach to engineer cartilage with porous bacterial nanocellulose for reconstruction of a human auricle. J Biomater Appl 28:626–640. https://doi.org/10.1177/0885328212472547

Gama M, Gatenholm P, Klemm D (2013) Bacterial nanocellulose: a sophisticated multifunctional material. CRC Press Taylor & Francis Group, Boca Raton

Gao Y (2017) Biology of vascular smooth muscle: vasoconstriction and dilatation. Springer, Singapore

George J, Ramana KV, Bawa AS (2011) Bacterial cellulose nanocrystals exhibiting high thermal stability and their polymer nanocomposites. Int J Biol Macromol 48:50–57. https://doi.org/10.1016/j.ijbiomac.2010.09.013

Gershlak JR, Hernandez S, Fontana G, Perreault LR, Hansen KJ, Larson SA, Binder BY, Dolivo DM, Yang T, Dominko T, Rolle MW, Weathers PJ, Medina-Bolivar F, Cramer CL, Murphy WL, Gaudette GR (2017) Crossing kingdoms: using decellularized plants as perfusable tissue engineering scaffolds. Biomaterials 125:13–22. https://doi.org/10.1016/j.biomaterials.2017.02.011

Giraud S, Favreau F, Chatauret N, Thuillier R, Maiga S, Hauet T (2011) Contribution of large pig for renal ischemia-reperfusion and transplantation studies: the preclinical model. J Biomed Biotechnol 2011:532127. https://doi.org/10.1155/2011/532127

Góra A, Pliszka D, Mukherjee S, Ramakrishna S (2016) Tubular tissues and organs of human body—challenges in regenerative medicine. J Nanosci Nanotechnol 16:19–39. https://doi.org/10.1166/jnn.2016.11604

Gueutin V, Deray G, Isnard-Bagnis C (2012) Renal physiology. Bull Cancer 99:237–249. https://doi.org/10.1684/bdc.2011.1482

Hagens G, Tiedemann K, Kriz W (1987) The current potential of plastination. Anat Embryol 175:411–421. https://doi.org/10.1007/bf00309677

Huling J, Min SI, Kim DS et al (2019) Kidney regeneration with biomimetic vascular scaffolds based on vascular corrosion casts. Acta Biomater 95:328–336. https://doi.org/10.1016/j.actbio.2019.04.001

Huntley CJ, Crews KD, Abdalla MA, Russell AE, Curry ML (2015) Influence of strong acid hydrolysis processing on the thermal stability and crystallinity of cellulose isolated from wheat straw. Int J Chem Eng 2015:1–11. https://doi.org/10.1155/2015/658163

Iguchi M, Yamanaka S, Budhiono A (2000) Bacterial cellulose—a masterpiece of nature's arts. J Mater Sci 35:261–270. https://doi.org/10.1023/A:1004775229149

Imai T, Sugiyama J (1998) Nanodomains of I α and I β cellulose in algal microfibrils. Macromolecules 31:6275–6279. https://doi.org/10.1021/ma980664h

Isogai A (2013) Wood nanocelluloses: fundamentals and applications as new bio-based nanomaterials. J Wood Sci 59:449–459. https://doi.org/10.1007/s10086-013-1365-z

Kc N, Priya K, Lama S, Magar A (2007) Plastination—an unrevealed art in the medical science. Kathmandu Univ Med J 5:139–141

Kim J, Cai Z, Lee HS, Choi GS, Lee DH, Jo C (2011) Preparation and characterization of a bacterial cellulose/chitosan composite for potential biomedical application. J Polym Res 18:739–744. https://doi.org/10.1007/s10965-010-9470-9

Lei D, Yang Y, Liu Z et al (2019) 3D printing of biomimetic vasculature for tissue regeneration. Mater Horiz 6:1197–1206. https://doi.org/10.1039/c9mh00174c

Levey AS, Eckardt KU, Tsukamoto Y, Levin A, Coresh J, Rossert J, De Zeeuw D, Hostetter TH, Lameire N, Eknoyan G (2005) Definition and classification of chronic kidney disease: a position statement from kidney disease: improving global outcomes (KDIGO). Kidney Int 67:2089–2100. https://doi.org/10.1111/j.1523-1755.2005.00365.x

Li S, Cui C, Hou H, Wu Q, Zhang S (2015) The effect of hyperbranched polyester and zirconium slag nanoparticles on the impact resistance of epoxy resin thermosets. Composites B 79:342–350

McMurry J (2004) Q Organica. Thomson, Mexico

Molina-Ramirez C, Castro M, Osorio M et al (2017) Effect of different carbon sources on bacterial nanocellulose production and structure using the low pH resistant strain *Komagataeibacter medellinensis*. Materials 10:1–12. https://doi.org/10.3390/ma10060639

Murphy SV, Atala A (2014) 3D bioprinting of tissues and organs. Nat Biotechnol 32:773–785. https://doi.org/10.1038/nbt.2958

Osorio M, Velásquez-Cock J, Restrepo LM, Zuluaga R, Gañán P, Rojas OJ, Ortiz-Trujillo I, Castro C (2017) Bioactive 3D-shaped wound dressings synthesized from bacterial cellulose: effect on cell adhesion of polyvinyl alcohol integrated in situ. Int J Polym Sci 2017:1–10. https://doi.org/10.1155/2017/3728485

Osorio M, Fernández-Morales P, Gañán P et al (2018) Development of novel three-dimensional scaffolds based on bacterial nanocellulose for tissue engineering and regenerative medicine: effect of processing methods, pore size and surface area. J Biomed Mater Res Part A 107:348–359. https://doi.org/10.1002/jbm.a.36532

Osorio M, Cañas A, Puerta J et al (2019a) Ex vivo and in vivo biocompatibility assessment (blood and tissue) of three-dimensional bacterial nanocellulose biomaterials for soft tissue implants. Sci Rep 9:1–14. https://doi.org/10.1038/s41598-019-46918-x

Osorio M, Ortiz I, Gañán P et al (2019b) Novel surface modification of three-dimensional bacterial nanocellulose with cell-derived adhesion proteins for soft tissue engineering. Mater Sci Eng C 100:697–705. https://doi.org/10.1016/j.msec.2019.03.045

Petrochenko PE, Torgersen J, Gruber P, Hicks LA, Zheng J, Kumar G, Narayan RJ, Goering PL, Liska R, Stampfl J, Ovsianikov A (2015) Laser 3D printing with sub-microscale resolution of porous elastomeric scaffolds for supporting human bone stem cells. Adv Healthc Mater 4:739–747. https://doi.org/10.1002/adhm.201400442

Recouvreux DOS, Rambo CR, Berti FV, Carminatti CA, Antônio RV, Porto LM (2011) Novel three-dimensional cocoon-like hydrogels for soft tissue regeneration. Mater Sci Eng C 31:151–157. https://doi.org/10.1016/j.msec.2010.08.004

Rouwkema J, Rivron NC, van Blitterswijk CA (2008) Vascularization in tissue engineering. Trends Biotechnol 26:434–441. https://doi.org/10.1016/j.tibtech.2008.04.009

Rueden CT, Schindelin J, Hiner MC, DeZonia BE, Walter AE, Arena ET, Eliceiri KW (2017) Image J2: ImageJ for the next generation of scientific image data. BMC Bioinformatics 18:529. https://doi.org/10.1186/s12859-017-1934-z

Shi Z, Zang S, Jiang F, Huang L, Lu D, Ma Y, Yang G (2012) In situ nano-assembly of bacterial cellulose–polyaniline composites. RSC Adv 2:1040–1046. https://doi.org/10.1039/C1RA00719J

Shimazono Y (2007) The state of the international organ trade: a provisional picture based on integration of available information. Bull World Health Organ 85:955–962. https://doi.org/10.2471/blt.06.039370

Su X, Zhao Q, Zhang D, Dong W (2015) Synthesis and membrane performance characterization of self-emulsified waterborne nitrocellulose dispersion modified with castor oil. Appl Surf Sci 356:610–614. https://doi.org/10.1016/j.apsusc.2015.08.108

Sullivan F, Simon L, Loannidis N, Patel S, Ophir Z, Gogos C, Jaffe M, Tirmizi S, Bonnett P, Abbate P (2018) Nitration kinetics of cellulose fibers derived from wood pulp in mixed acids. Ind Eng Chem Res 57:1883–1893. https://doi.org/10.1021/acs.iecr.7b03818

UNOS (2018) National Data UNOS. https://unos.org/data/. Accessed 9 Apr 2018

von Hagens G (1979) Impregnation of soft biological specimens with thermosetting resins and elastomers. Anat Rec 194:247–255. https://doi.org/10.1002/ar.1091940206

Wang H, Liu Y, Li M, Huang H, Xu HM, Hong RJ, Shen H (2010) Multifunctional TiO_2 nanowires-modified nanoparticles bilayer film for 3D dye-sensitized solar cells. Optoelectron Adv Mater Rapid Commun 4:1166–1169

Yan Z, Chen S, Wang H, Wang B, Jiang J (2008) Biosynthesis of bacterial cellulose/multi-walled carbon nanotubes in agitated culture. Carbohydr Polym 74:659–665. https://doi.org/10.1016/j.carbpol.2008.04.028

Yeong WY, Sudarmadji N, Yu HY, Chua CK, Leong KF, Venkatraman SS, Boey YC, Tan LP (2010) Porous polycaprolactone scaffold for cardiac tissue engineering fabricated by selective laser sintering. Acta Biomater 6:2028–2034. https://doi.org/10.1016/j.actbio.2009.12.033

Zhu C, Fan D, Wang Y (2014) Human-like collagen/hyaluronic acid 3D scaffolds for vascular tissue engineering. Mater Sci Eng C 34:393–401. https://doi.org/10.1016/j.msec.2013.09.044